Identification of neoadjuvant chemoradiotherapy resistance-associated proteins in locally advanced rectal cancer: A pilot study

JIANG-YI HE[1*], YAN DONG[1*], CAN CHEN[1*], FANG-HAO LU[1], FENG-WEI RAN[1], QIONG DING[1], YUN DU[1], TAO-RUI LIU[1], YU-YING ZHANG[1], TENG WANG[1], YU-HAN CHEN[1], XIANG ZHAO[1], SEN-LIN XU[2] and JIAN-JUN LI[1]

[1]Department of Oncology and Southwest Cancer Center, Southwest Hospital, Third Military Medical University (Army Medical University), Chongqing 400038, P.R. China; [2]Department of Pathology, Southwest Hospital, Third Military Medical University (Army Medical University), Chongqing 400038, P.R. China

Received February 18, 2026; Accepted May 28, 2026

DOI: 10.3892/ol.2026.15722

Abstract. Neoadjuvant chemoradiotherapy (nCRT) resistance in locally advanced rectal cancer (LARC) leads to worse outcomes. The present pilot study aimed to identify candidate proteins associated with resistance to nCRT. Data-independent acquisition mass spectrometry on 15 formalin-fixed paraffin-embedded tumor tissues, collected before and after nCRT, from four nCRT-resistant and four nCRT-sensitive LARC cases, was performed, identifying 6,006 proteins. Before nCRT, 133 proteins were found to be more abundant in resistant tumors and were preliminarily enriched in cell junction and metabolic pathways. After nCRT, 290 proteins were found to be more abundantly expressed in resistant tumors and were preliminarily enriched in pathways associated with DNA replication, transcription, translation and metabolism. Combined analysis of datasets GSE209746 and PXD060201 prioritized branched-chain keto acid dehydrogenase E1 subunit α (BCKDHA) as a candidate resistance-associated protein. In a colorectal cancer (CRC) tissue microarray, upregulated BCKDHA expression was associated with shorter overall survival, supporting its broader clinical relevance in CRC. In SW480 cells, BCKDHA overexpression increased clonogenic survival following irradiation, whereas BCKDHA knockdown enhanced radiosensitivity. These changes were accompanied by altered ataxia telangiectasia mutated, checkpoint kinase 2, DNA repair protein RAD51 homolog 1-associated signaling and γ-H2A histone family member X dynamics after irradiation. Collectively, these data identified BCKDHA as a candidate nCRT resistance-associated protein in LARC and provided preliminary functional evidence associating BCKDHA with the response to radiotherapy and DNA damage response-associated signaling. Further validation in larger pretreatment LARC cohorts and more direct mechanistic studies is warranted.

Introduction

Colorectal cancer (CRC) is the third most common malignancy and the second leading cause of cancer-related mortality worldwide (1). In China, CRC has the second-highest prevalence (after lung cancer) and is the fourth leading cause of cancer-associated mortalities; of these CRC cases, 49.8% are rectal cancer (2). Neoadjuvant chemoradiotherapy (nCRT) is a preoperative treatment for rectal cancer, particularly middle and low locally advanced rectal cancer (LARC) and is considered the standard neoadjuvant treatment (3,4). Complete tumor regression following nCRT is associated with favorable survival outcomes (5). However, the response to nCRT is heterogeneous, with 12-18% of cases developing a pathological complete response rate (6,7), whereas 11-20% of cases develop progressive disease (PD) (8,9). Therefore, the molecular signatures of nCRT-resistant LARC require further investigation, providing insights for identifying potential predictive biomarkers and candidate therapeutic targets to enhance the precision treatment of LARC.

Owing to advancements in sequencing technologies, numerous studies have reported the molecular features of nCRT resistance in LARC. KRAS, neuroblastoma RAS viral

Correspondence to: Dr Jian-Jun Li, Department of Oncology and Southwest Cancer Center, Southwest Hospital, Third Military Medical University (Army Medical University), 30 Gaotanyan Street, Chongqing 400038, P.R. China
E-mail: jianjunli@tmmu.edu.cn

Dr Sen-Lin Xu, Department of Pathology, Southwest Hospital, Third Military Medical University (Army Medical University), 30 Gaotanyan Street, Chongqing 400038, P.R. China
E-mail: xusenlin@tmmu.edu.cn

*Contributed equally

Key words: locally advanced rectal cancer, neoadjuvant chemoradiotherapy, therapy resistance, data-independent acquisition mass spectrometry, branched-chain keto acid dehydrogenase E1 subunit α

oncogene homolog and BRAF mutations are associated with poor tumor downstaging (10-12). A genome-based model for adjusting the radiotherapy dose has been the best-recognized predictive model for radiosensitivity. The genomic-adjusted radiation dose (GARD) model has been proposed as a genome-based approach for estimating the biological effect of radiotherapy. GARD is derived by integrating the gene-expression-based radiosensitivity index, which is based on a 10-gene signature (androgen receptor, c-Jun, STAT1, protein kinase C, RELA proto-oncogene, NF-κB subunit, cABL, small ubiquitin-like modifier 1, CDK1, histone deacetylase 1 and interferon regulatory factor 1), with the linear quadratic model (13). In rectal cancer, GARD values >17 are associated with improved therapeutic effects (14). An additional RNA sequencing study of 114 pre-treatment LARC biopsies revealed that insulin-like growth factor 2 and L1 cell adhesion molecule (L1CAM) upregulation was associated with a worse nCRT response (15).

With regard to protein levels, studies have examined both circulating and tumor tissues to gain further insights (16-24). Serum samples, collected before and after nCRT, have been analyzed using techniques including matrix-assisted laser desorption/ionization time-of-flight (16) and isobaric tags for relative and absolute quantitation (iTRAQ) (17), revealing activated immune pathways in non-responders. Protein signatures in rectal cancer biopsies were initially detected using phosphorylated protein microarrays (18). Subsequent studies have used label-free liquid chromatography mass spectrometry (LC-MS) (19,20), isobaric tagging MS (21) and data-independent acquisition (DIA)-MS to identify additional potential biomarkers (22). For rectal tumor tissues before and after nCRT, a study analyzing samples using iTRAQ MS revealed that acid ceramidase was associated with the nCRT response (23). An additional study analyzed samples using label-free LC-MS, suggesting that ADAM metallopeptidase domain 10 and carbamoyl-phosphate synthetase 2, aspartate transcarbamylase and dihydroorotase were associated with nCRT response (24).

Despite the presence of DNA, RNA and proteomic studies predicting nCRT responses, the selected potential biomarkers are distinct among studies. This could be due to the inherent heterogeneity of human cancer types and variations in the tumor stage at diagnosis. Therefore, investigating the protein signatures of nCRT-resistant LARC is worthwhile. In the present pilot study, biopsy and resection tumor tissues were collected from four nCRT sensitive and four resistant patients with LARC and subjected to DIA-MS and combined with results of GSE209746 (15) and PXD060201 (25) dataset analysis. Therefore, the aim of the present study was to identify potential candidate biomarkers and therapeutic targets for nCRT resistance.

Materials and methods

Tissue sample collection. Formalin-fixed paraffin-embedded (FFPE) tumor tissue samples from 4 neoadjuvant treatment-sensitive and 4 treatment-resistant patients with LARC (T3-4N0 or any T, N+) who were treated at The First Affiliated Hospital of Army Medical University (Chongqing, China) between July 2018 and August 2022 were included in the present study. The cohort comprised of 7 men and 1 woman, with a median age of 64 years (range: 42-81 years). From retrospectively screened cases with pelvic MRI available both before and after nCRT, cases with clear radiological response categories according to Response Evaluation Criteria in Solid Tumors (RECIST) version 1.1 (https://project.eortc.org/recist/wp-content/uploads/sites/4/2015/03/RECISTGuidelines.pdf) and with adequate available FFPE material for pilot DIA-MS analysis were identified. The tumor staging was recorded according to the 8th edition of the American Joint Committee on Cancer (and Union for International Cancer Control Staging System for Colorectal Cancer) (26). Tumor response was evaluated 4-8 weeks after treatment according to the RECIST guidelines. Complete response (CR) and partial response (PR) were categorized as treatment-sensitive, whereas stable disease (SD) and PD were categorized as treatment-resistant. Response categories in the proteomic discovery set were defined primarily according to RECIST guidelines, using pelvic MRI before and after nCRT. Pathological tumor regression grade was recorded descriptively when available but was not used for the primary response grouping. Biopsy tissues were collected before neoadjuvant treatment and tumor tissues were collected during surgery after neoadjuvant therapy. The present study was conducted in accordance with the principles of the Declaration of Helsinki and was approved by the Ethics Committee of the First Affiliated Hospital of Army Medical University, PLA [approval no. (A)KY2025105]. Written informed consent was obtained from all participants or their legal guardians, where applicable.

Pre-nCRT biopsy samples were obtained through colonoscopic biopsy. Fresh samples were fixed in 10% neutral buffered formalin at room temperature for 12-24 h, followed by routine pathological examination whereby ~4 μm sections were cut from FFPE blocks and stained with H&E for pathological determination of adenocarcinoma.

Post-nCRT samples were fresh, unfixed and uncut. After collection, images of gross samples were routinely captured and sectioned. To accurately assess tumor regression and account for intratumoral heterogeneity post-treatment, the entire tumor was sampled. All specimens were fixed in 10% neutral buffered formalin (Chongqing Boyi Chemical Reagent Co., Ltd.) at room temperature for 24-48 h, sectioned for routine histopathological examination and 4 μm FFPE sections were stained with H&E for analysis.

H&E staining of both pre-nCRT biopsy specimens and post-nCRT resection specimens was performed using the same staining program on an automated slide stainer (Ningbo Chiwell Biotechnology Co., Ltd.) at room temperature. Briefly, FFPE sections were deparaffinized in xylene, rehydrated through graded ethanol and water, stained with hematoxylin for 5 min, differentiated for 8 sec, blued for 15 sec and counterstained with eosin for 7 sec. All H&E-stained sections from both pre-nCRT biopsy specimens and post-nCRT resection specimens were visualized using an Olympus BX43 microscope (Olympus Corporation).

Protein extraction from FFPE tissue samples, digestion and preparation. For 15 FFPE rectal cancer tissues from 8 patients (8 before and 7 post-nCRT treatment), 8 sections (10-μm thick) were cut using a microtome and transferred to 5 ml Eppendorf

tubes. Before protein extraction, FFPE sections were reviewed by an experienced pathologist, but no macrodissection or laser-capture microdissection was performed. Proteins were extracted using an EasyPept FFPE micro sample preparation kit (cat. no. OSFP0006; Shanghai Omicsolution Co., Ltd.). Briefly, tissue sections were lysed using 50 μl kit-provided lysis buffer with steel balls and subjected to 55 Hz grinding for 4 min at 4˚C; the samples were then incubated with agitation at 95˚C and 1,000 rpm for 30 min. The sample was left to stand and after it reached room temperature, the supernatant was collected after centrifugation (4˚C; 12,000 x g; 20 min) and the protein concentration was determined using the BCA method. A total of 30 μg of protein was incubated at 95˚C for 2 h for reduction and alkylation and cooled to room temperature. The samples were then digested with the kit-provided protease at 37˚C for 3 h, after which it was centrifuged (room temperature; 20,000 x g; 1 min) and the supernatant was collected. The peptide-containing supernatant was loaded onto a desalting column. The column was then washed twice and peptides were eluted with 100 μl kit-provided elution buffer, which was then dried using a JM50-Plus vacuum freeze dryer (Beijing JM Technology Co., Ltd.) for subsequent analysis.

Nano-LC-MS/MS analysis. For each sample, 200 ng total peptide was mixed with a kit containing 11 standard peptides (cat. no. Ki-3002-2; Biognosys AG) at a 1:10 ratio, then separated using a nanoElute LC system (Bruker Daltonics GmbH). Peptides were first trapped on a thermo trap cartridge using mobile phase A (0.1% formic acid in water) and then separated on a 15 cm reversed-phase C18 PepSep® column (Bruker Daltonics GmbH; particle size: 1.9 μm; inner diameter: 75 μm) maintained at 50˚C. Gradient elution was performed at a flow rate of 0.3 μl/min: Mobile phase B proportion (0.1% formic acid in acetonitrile) increased from 2 to 24% in the first 30 min, then to 38% in the next 5 min and to 80% in 7 min (total duration: 42 min) and finally maintained at 80% for 3 min.

Ultra-high-performance LC was coupled to a timsTOF Pro2 mass spectrometer (Bruker Daltonics GmbH) equipped with a nano-electrospray ion source operated in positive ion mode. The nitrogen gas temperature was set to 180˚C, the nebuliser pressure was 2.90 psi and the dry gas flow rate was 3.0 l/min. Data were acquired in Parallel Accumulation-Serial Fragmentation mode. The electrospray ion source voltage was set to 1,400 V, precursor scanning range was 100-1,700 m/z, ion mobility range (1/K0) was 0.6-1.6 Vs/cm^2 and both trapped ion mobility spectrometry ramp time and accumulation time were set to 100 ms, with a duty cycle close to 100%. The secondary mass spectrometry scanning range was 400-1,200 m/z and the collision energy increased linearly with ion mobility (20 eV at 0.85 Vs/cm^2 and 59 eV at 1.3 Vs/cm^2). The isolation window was set to 25 Th, with a total of 32 windows.

Protein identification and quantitation. Raw MS files were processed in library-free mode using Spectronaut® software (version 18.2.230802.50606; Biognosys AG) with its built-in Pulsar search engine. MS spectra lists were searched against their species-level UniProt FASTA database (uniprot_Homo sapiens_9606_reviewed_2024_05_fasta, https://www.uniprot.org/proteomes/UP000005640), with carbamidomethylation of cysteine as a fixed modification and oxidation of methionine and acetylation of protein N-termini as variable modifications. Trypsin was used as the protease. A maximum of two missed cleavages was allowed. The false discovery rate at both peptide and protein levels was set to 0.01. The maximum allowable initial precursor mass deviation for peptide identification was 20 ppm and the maximum allowable fragment mass deviation was 20 ppm. The raw data screening criterion was that each protein contained at least 1 unique peptide. Since samples were collected both before and after treatment, protein abundance may have been downregulated; thus, missing values were replaced with half of the detected minimum value.

Bioinformatic analysis. Bioinformatic analyses were performed using R software (version 3.6.3; R Foundation for Statistical Computing) (27). Principal component analysis (PCA) was performed using the R package 'ropls' (version 1.16.0) (28) and visualized using 'ggplot2' (version 3.3.2) (29). Proteins were considered differentially abundant proteins (DAPs) if they met a nominal $P<0.05$ by Student's t-test and had a fold change ≥ 1.2 or ≤ 0.83. DAPs were visualized using bar plots generated with 'ggplot2'. Hierarchical clustering heatmaps were generated using 'pheatmap' (version 1.0.12) (30). Subcellular localization analysis was performed using 'loctree3' (version 1.0.1) (31) and visualized using 'ggplot2'. Kyoto Encyclopedia of Genes and Genomes (KEGG) pathway analysis was performed using the KEGG database (http://rest.kegg.jp) (32) and the results were visualized using 'ggplot2'. The public transcriptomic dataset GSE209746 (https://www.ncbi.nlm.nih.gov/geo/query/acc.cgi?acc=GSE209746) (15) and public proteomic dataset PXD060201 (https://www.ebi.ac.uk/pride/archive/projects/PXD060201) (25) were downloaded and analyzed for cross-dataset prioritization of candidate proteins associated with nCRT response.

Immunohistochemistry (IHC) and assessment of immunostaining intensity. For IHC experiments, a tissue microarray (TMA) containing 92 CRC and 87 matched adjacent non-tumor tissues was acquired from Shanghai Outdo Biotech Co., Ltd. (cat. no. HColA180Su24). IHC staining was conducted using an IHC SP Kit (cat. no. SP-9001; Beijing Zhongshan Jinqiao Biotechnology Co., Ltd.) following the manufacturer's instructions. The primary antibody used was anti-branched-chain keto acid dehydrogenase E1 subunit α (BCKDHA; cat. no. 30028-1-AP; 1:6,000; Proteintech Group, Inc.) overnight at 4˚C. Staining results were assessed independently by two pathologists. Staining intensity was classified into four levels: Negative, score 0; weak, score 1; medium, score 2; and strong, score 3. The percentage of positively stained cells ranged from 0-100%. The final IHC score was calculated by multiplying the percentage of positive cells by the staining intensity. High and low BCKDHA expression were defined using an IHC score cut-off of 2.375; scores ≤2.375 were classified as low expression, whereas scores >2.375 were classified as high expression.

Cell culture. The human CRC SW480 cell line was obtained from American Type Culture Collection (cat. no. CCL-228), grown in medium supplemented with 10% FBS (Sangon Biotech Co., Ltd.) and maintained in a humidified 5% CO_2 incubator at 37˚C, with cells passaged using standard cell culture techniques.

Generation of stable cell lines. To construct the BCKDHA-overexpressing cell lines, the BCKDHA coding sequence was synthesized by Beijing Tsingke Biotech Co., Ltd., and then inserted into the XhoI-NotI sites of the pLV10ltr-PGK-Hyg-CMV vector (Beijing Tsingke Biotech Co., Ltd.). The short hairpin (sh-)RNAs were integrated into the pLKO.1-mCherry-puro vector (Beijing Tsingke Biotech Co., Ltd.). The scrambled RNA sequence was 3'-CCGGGG TTCTCCGAACGTGTCACGTCTCGAGACGTGACACGT TCGGAGAACCTTTTTT-5' and the shBCKDHA sequence was 3'-CCGGGGGTATGGCATCATGTCAATCCTCGA GGATTGACATGATGCCATACCCTTTTTT-5'. For lentiviral packaging, 5 μg transfer plasmid was co-transfected with 3.5 μg psPAX2 and 1.5 μg pMD2.G plasmids into 293T cells in 6-cm dishes using polyethylenimine (Yeasen Biotechnology Co., Ltd.). The plasmid-PEI complexes were formed at room temperature for 15 min and then added to 293T cells. After incubation at 37˚C for 48 h, the supernatant was harvested and used to infect SW480 cells. SW480 cells were screened using 200 μg/ml hygromycin for 7 days or 3 μg/ml puromycin for 3 days. The construct efficiency was determined using a western blotting.

X-ray irradiation. For the colony formation assay and western blotting analyses after irradiation, cells were seeded into 6-well plates in 2 ml DMEM supplemented with 10% FBS (both Sangon Biotech Co., Ltd.). Irradiation was performed using a Varian 600CD machine (Varian Medical Systems, Inc.) with 6 MV X-rays at a dose rate of 4 Gy/min. The source-to-surface distance was set to 100 cm with a field size of 37.0x39.4 cm. For dose buildup, the plates were covered with 1 cm solid water and placed on a 4 cm-thick solid water slab beneath. Irradiation was delivered at a gantry angle of 0˚.

Colony formation assay. SW480 cells were seeded at 1,000 or 2,000 cells per well in 6-well plates. The following day, cells were exposed to 0, 1, 2, 3, 4 or 5 Gy radiation at a dose rate of 4 Gy/min at room temperature, corresponding to irradiation durations of 0, 15, 30, 45, 60 and 75 sec, respectively. Cells were then cultured in a humidified 5% CO_2 incubator at 37˚C for 10-14 days to allow colony formation. Colonies were fixed with 4% formaldehyde at room temperature for 20 min, stained with 0.05% crystal violet, and analyzed using ImageJ (version 1.54 g; National Institutes of Health). Colonies containing >50 cells were considered surviving colonies. The survival fraction was calculated as follows: Planting efficiency (PE) of untreated (UT) cells (PE_{UT})=(number of colonies/number of seeded cells) x100; survival fraction=number of colonies/(number of seeded cells x PE_{UT}/100).

Western blotting. Western blotting analysis was performed as previously described (33). In brief, cells were lysed in RIPA buffer (cat. no. C510006; Sangon Biotech Co., Ltd.) containing a protease inhibitor (Roche Diagnostics GmbH) and incubated on a rocker at 4˚C for 15 min. The protein concentration of the lysates was measured using a BCA protein kit (Sangon Biotech Co., Ltd.), normalized to equal amounts of protein (20 μg per lane), resolved on a 10-12% SDS-gel, transferred to PVDF membranes and probed at 4˚C overnight with one of the following primary antibodies: BCKDHA (cat. no. A21588; 1:1,000), phosphorylated (p)-ataxia telangiectasia mutated (p-ATM; Ser1981; cat. no. AP1030; 1:500), ATM (cat. no. A19650; 1:500), p-checkpoint kinase 2 (p-Chk2; Thr68; cat. no. AP0590; 1:1,000), Chk2 (cat. no. A19543; 1:500), DNA repair protein RAD51 homolog 1 (RAD51; cat. no. A26856; 1:1,000), H2A histone family member X (γ-H2AX; cat. no. AP1555; 1:1,000), H2AX (cat. no. A11361; 1:1,000) or β-actin (cat. no. AC026, 1:1,000). All primary antibodies were purchased from ABclonal Biotech Co., Ltd. After probing with HRP-conjugated goat anti-rabbit IgG (cat. no. D110058; 1:2,500) or HRP-conjugated goat anti-mouse IgG (cat. no. D110087; 1:2,500) secondary antibodies (both Sangon Biotech Co., Ltd.) at room temperature for 1 h, signals were detected using an ECL reagent (cat. no. C520045; Sangon Biotech Co., Ltd.).

Statistical analysis. A χ^2 test was used to assess the association between BCKDHA expression and clinicopathological parameters. Kaplan-Meier analysis and the log-rank test were performed to assess the association between BCKDHA expression and overall survival (OS) in patients with CRC. Multivariate survival analysis was performed using Cox proportional hazards regression analysis. The survival fraction in the colony formation assay was analyzed for significance using two-way ANOVA. $P<0.05$ was considered to indicate a statistically significant difference.

Results

Clinical characteristics of patients based on the proteomics analysis. To investigate proteins potentially associated with nCRT response in LARC, four nCRT-sensitive and four nCRT-resistant FFPE tumor tissue pairs collected before and after treatment were analyzed using DIA-MS (Fig. 1A). The clinical characteristics of the 8 patients are summarized in Table I. Representative MRI images of one nCRT-sensitive case and one nCRT-resistant case before and after nCRT are shown in Fig. 1B. The patients received intensity-modulated radiation therapy (Fig. 1C) combined with concurrent capecitabine chemotherapy. After nCRT, all patients underwent surgery except one patient with PD, yielding 15 FFPE tumor specimens for proteomic analysis. Representative H&E staining is shown in Fig. 1D.

Proteomics analysis. DIA-MS identified 39,052 peptides and 6,006 proteins. Samples were labeled by treatment status and response: Before_sensitive (BS), before_resistant (BR), post_sensitive (PS) and post_resistant (PR). PCA revealed distinct separation among the four groups (Fig. 2A). Bar plots of DAPs are shown in Fig. 2B. To characterize response-associated DAPs, comparisons between BS with BR and PS with PR were performed. Under this denominator-first notation, a higher abundance in the second group corresponded to the resistant group in these two comparisons. Hierarchical clustering using proteins meeting the predefined thresholds separated sensitive and resistant samples both before treatment and after nCRT (Fig. 2C and D). The complete list of identified proteins and the DAP lists for the BS vs. BR and PS vs. PR comparisons are provided in Tables SI-III. Given this was a small proteomic discovery set, these analyses were intended for candidate prioritization rather than definitive biomarker selection.

Table I. Clinical characteristics.

Sample no.	1	2	3	4	5	6	7	8
Response status	S	S	S	S	R	R	R	R
Response evaluation	PR	PR	PR	PR	PD	PD	SD	SD
Mandard TRG	1	2	1	1	3	N/A	3	3
Sex	M	M	F	M	M	M	M	M
Age, years	64	81	46	64	43	68	64	42
Distance from anal verge, cm	3.8	8.3	4.2	4.5	5.4	7.2	1.6	4.2
cTNM	T4aN0	T4aN2b	T4aN2b	T4bN2b	T2N2a	T3bN2	T3bN2	T3bN2a
CRM	-	+	-	+	-	-	-	+
EMVI	-	+	+	+	-	+	+	-
ypTNM	T3N0	T3N1a	T3N0	T2N0	T3N1c	T4aN0	T3N0	T3N1c
Radiation dose, Gy	50.0	50.0	50.4	50.0	50.4	50.4	50.4	50.4
Fractions	25	25	28	25	28	28	28	28

TRG was recorded descriptively when available and was not used for the primary response grouping, which was based on Response Evaluation Criteria in Solid Tumors (version 1.1). N/A indicates that no surgical specimen was available for pathological TRG assessment. TRG, Tumor regression grade; M, male; F, female; T, tumor; N, node; CRM, circumferential resection margin; EMVI, extramural vascular invasion; PD, progressive disease; SD, stable disease; PR, partial response.

Preliminary pathway-level characterization of proteins more abundant in nCRT-resistant tumors. To identify candidate proteins associated with nCRT resistance, proteins that were more abundant in resistant than in sensitive tumors before nCRT (BS vs. BR) and after nCRT (PS vs. PR) were examined. Before nCRT, 133 proteins were found to be more abundant in resistant tumors, primarily localized in the cytoplasm (33.08%), secretory fraction (24.81%) and nucleus (24.06%; Fig. 3A). Preliminary KEGG analysis indicated enrichment in pathways that include 'Adherens junction', 'Focal adhesion', 'Tight junction', 'Regulation of actin cytoskeleton', 'Propanoate metabolism' and 'Amino sugar and nucleotide sugar metabolism' (Fig. 3B). After nCRT, 290 proteins were found to be more abundant in resistant tumors, with nuclear localization (36.55%) being the most prominent category (Fig. 3C). Preliminary enrichment was observed in pathways that include 'DNA replication', 'RNA polymerase', 'Ribosome', 'Protein export', 'Nucleocytoplasmic transport' and 'Metabolic pathways' (Fig. 3D). Representative proteins of interest from these comparisons are listed in Tables II and III.

Cross-dataset prioritization identifies BCKDHA as a candidate resistance-associated protein and CRC TMA supports its broader clinical relevance. To further prioritize candidate proteins associated with nCRT response, the public proteomic dataset PXD060201 (25) and transcriptomic dataset GSE209746 (15) were analyzed. BCKDHA emerged as a shared candidate across all three datasets (Fig. 4A). BCKDHA is the E1 subunit of the branched-chain keto acid dehydrogenase complex, which catalyzes the catabolism of branched-chain amino acids (34). In the present proteomic discovery set, BCKDHA exhibited higher abundance in resistant tumors both before and after nCRT (Fig. 4B and C). A similar direction of change was observed in PXD060201 (Fig. 4D) and GSE209746 (Fig. 4E).

To further assess its broader clinical relevance, IHC staining was performed on a TMA containing samples from 92 patients with CRC, with 87 matched adjacent non-tumorous tissues. BCKDHA localized to the cytoplasm (Fig. 4G) and IHC scores were significantly higher in CRC tissues compared with adjacent non-tumor tissues (Fig. 4F). The χ^2 test (Table IV) showed that high BCKDHA expression was significantly associated with patient age. Kaplan-Meier analysis showed that high BCKDHA expression was associated with shorter OS in patients with CRC (Fig. 4H). Cox proportional hazards regression analysis (Table V) revealed that high BCKDHA expression, pathology grade and T stage were significantly associated with worse OS in univariate analysis. Multivariate Cox regression showed that high BCKDHA expression was independently associated with a shorter OS in the CRC cohort. Collectively, these data support BCKDHA as a candidate protein associated with nCRT resistance and suggest broader clinical relevance in CRC.

Preliminary functional data support an association between BCKDHA and responses to radiotherapy and to DNA damage response (DDR)-associated signaling in SW480 cells. To examine whether BCKDHA contributed to the response to radiotherapy, SW480 cell lines with either stable BCKDHA overexpression or stable BCKDHA knockdown were established. In BCKDHA overexpressing SW480 cells, colony formation assays exhibited significantly increased survival after irradiation (Fig. 5A and B). In GSE209746, BCKDHA mRNA expression was found to be positively correlated with a number of DDR-associated genes, including ATM, ATR, BRCA1, BRCA2, RAD51, RAD52, RPA1, RPA2, RPA3, MRE11 and H2AX (Fig. 5C), supporting a potential association between BCKDHA and DDR. In BCKDHA-overexpressing SW480 cells, higher levels of ATM, Chk2, RAD51 and H2AX were observed, together with increased phosphorylation of ATM and Chk2 at 30 min to 1 h post-irradiation compared with

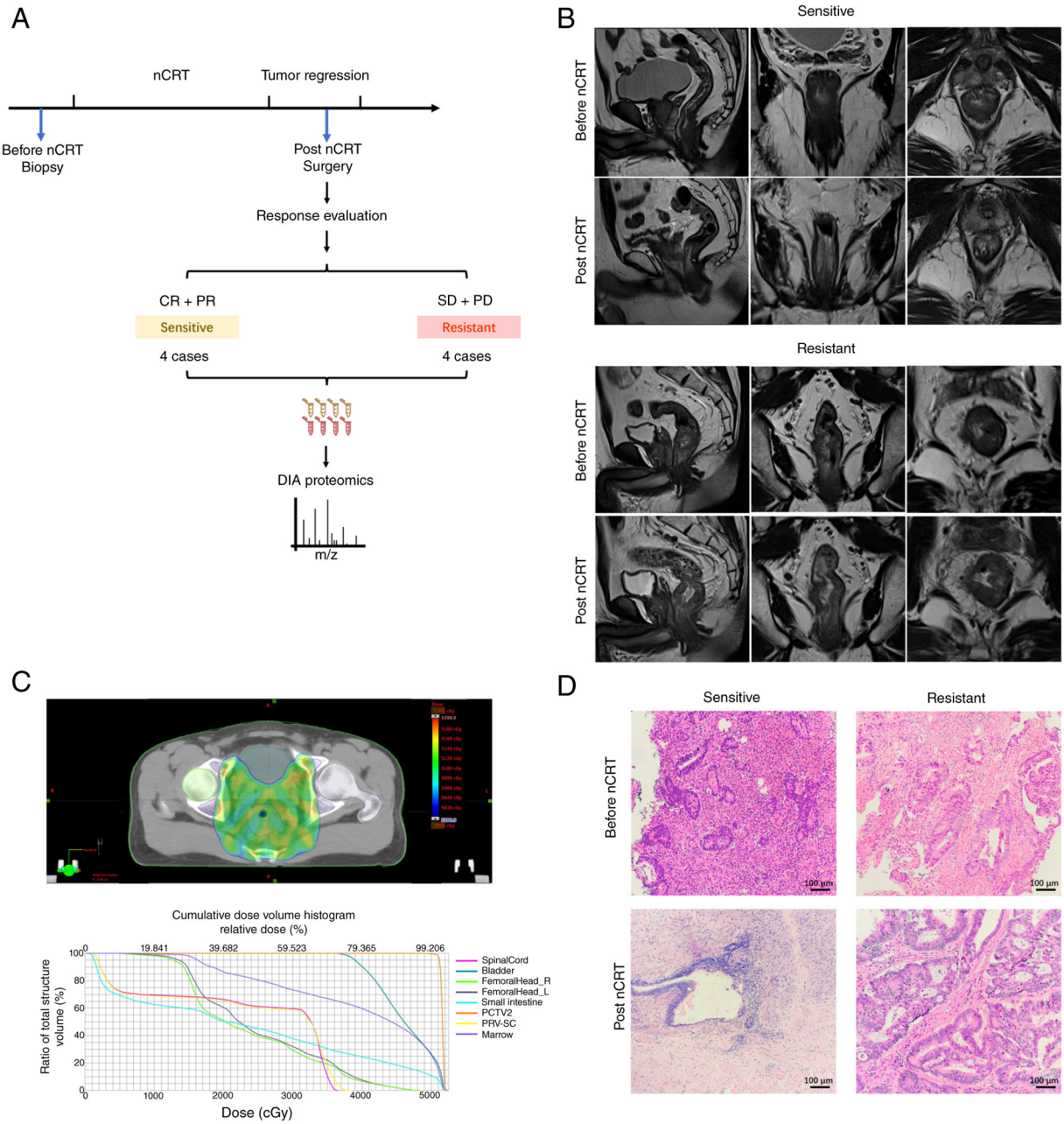

Figure 1. Selection of nCRT-sensitive and resistant patients with LARC for proteomic analysis. (A) Schematic diagram of the present study design and FFPE sample collection before and after nCRT, followed by DIA proteomics analysis. (B) Pelvic MRI images of representative nCRT-sensitive (upper panel) and resistant (lower panel) patients at baseline and post-nCRT. Sagittal (left), coronal (middle) and transverse (right) sections are shown. (C) Cumulative dose plan of intensity-modulated radiation therapy fractions (upper panel) and associated dose volume histogram (lower panel). (D) Representative H&E staining images (scale bar, 100 μm). Biopsy specimens before nCRT (upper panel) and resected tumor tissues after nCRT (lower panel; scale bar, 100 μm). nCRT, neoadjuvant chemoradiotherapy; LARC, locally advanced rectal cancer; FFPE, formalin-fixed paraffin-embedded; DIA, data-independent acquisition; PCTV2, planning clinical target volume 2; PRV-SC, planning organ at risk volume-spinal cord.

the control cells (Fig. 5D). In addition, BCKDHA overexpression was also accompanied by earlier induction of γ-H2AX after irradiation.

By contrast, stable BCKDHA knockdown significantly reduced colony formation after irradiation (Fig. 6A and B). BCKDHA knockdown was accompanied by lower levels of ATM, Chk2, RAD51 and H2AX, attenuated radiation-induced phosphorylation of ATM and Chk2 and lower γ-H2AX levels across the examined time points post-irradiation (Fig. 6C). Collectively, these findings provide preliminary functional evidence that BCKDHA overexpression is associated with increased clonogenic survival and a more resistant phenotype after irradiation, whereas BCKDHA knockdown is associated with reduced clonogenic survival and enhanced radiosensitivity in SW480 cells.

Discussion

In the present pilot study, DIA-MS was used to profile FFPE tumor specimens collected before and after nCRT from four cases each of sensitive and resistant LARC. A total of 6,006 proteins were identified as potentially relevant and used

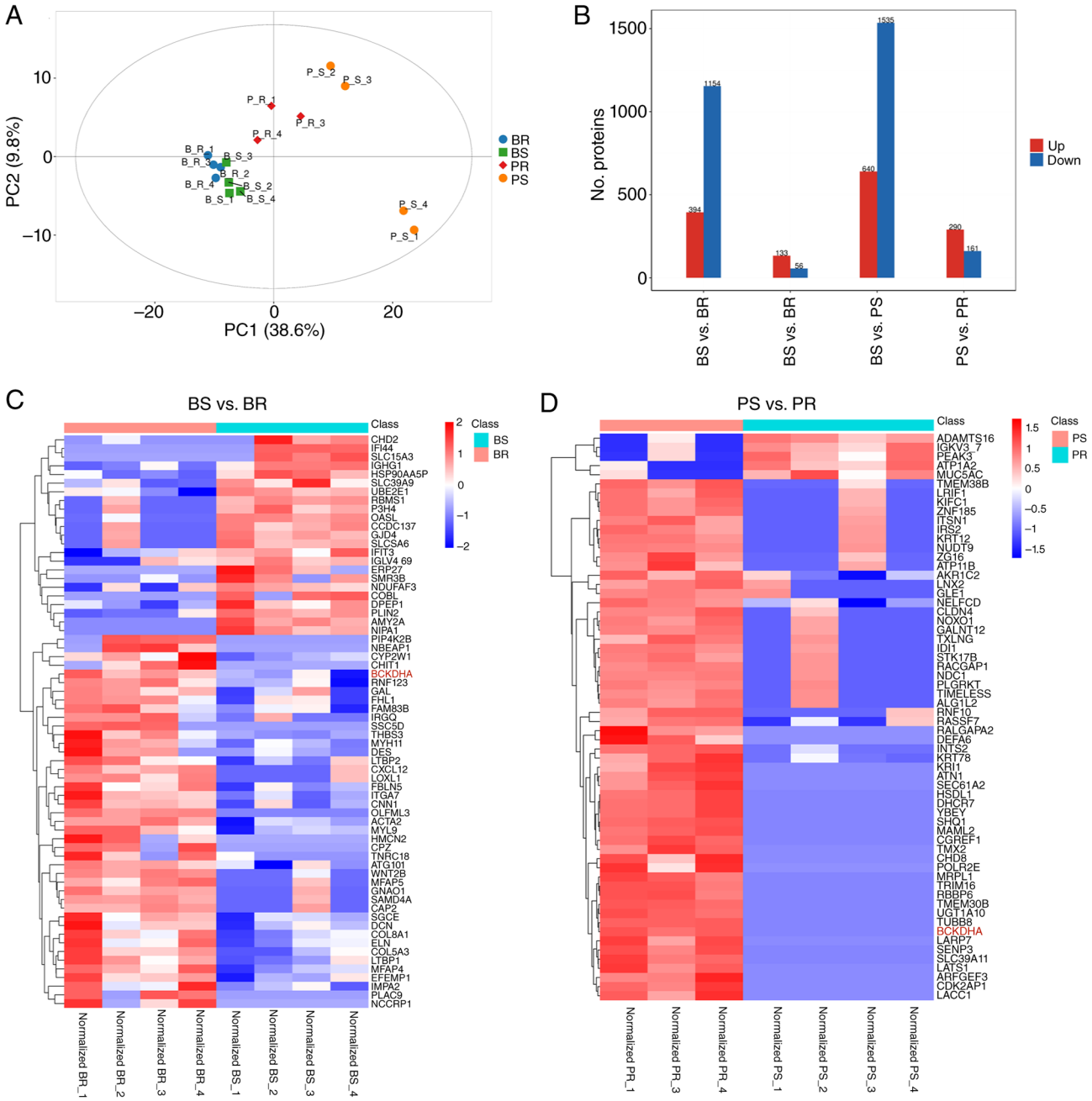

Figure 2. Overview of the proteomic profiling results. (A) Principal components analysis identified proteins in each group. Green, BS; blue, BR; orange, PS; and red, PR. (B) Bar plot showing the number of DAPs in the four indicated comparisons: BR vs. PR, BS vs. BR, BS vs. PS and PS vs. PR. DAPs were defined as those with P<0.05 (Student's t-test) and a fold change of ≥1.2 (upregulated, red) or ≤0.83 (downregulated, blue). In this denominator-first notation, red indicates higher abundance in the second group of each comparison and blue indicates higher abundance in the first group. Hierarchical clustering analysis of DAPs in comparison to (C) BS vs. BR and (D) PS vs. PR. Each row represents a protein and each column represents a sample. The relative protein abundance is shown as a Z-score, with red indicating upregulation and blue indicating downregulation. BS, sensitive before nCRT; BR, resistant before nCRT; PS, sensitive post-nCRT; PR, resistant post-nCRT; DAP, differentially abundant protein; nCRT, neoadjuvant chemoradiotherapy; Up, upregulated; Down, downregulated.

in a small proteomic discovery set to prioritize candidate proteins associated with response categories. Before nCRT, proteins more abundant in resistant tumors were preliminarily enriched in pathways such as 'Adherens junction', 'Focal adhesion', 'Tight junction', 'Regulation of actin cytoskeleton', 'Propanoate metabolism' and 'Amino sugar and nucleotide sugar metabolism'. After nCRT, proteins more abundant in resistant tumors were preliminarily enriched in pathways such as 'DNA replication', 'RNA polymerase', 'Ribosome', 'Protein export', 'Nucleocytoplasmic transport' and 'Metabolic pathways'. Cross-dataset comparison prioritized BCKDHA as a candidate resistance-associated protein and CRC TMA analysis showed that high BCKDHA expression was associated with shorter OS. In parallel, BCKDHA overexpression and knockdown experiments in SW480 cells provided preliminary functional evidence associating BCKDHA with the response to radiotherapy and to a number of DDR-associated proteins and signaling changes.

Prior to nCRT, the pathways preliminarily enriched in resistant tumors in the present small discovery set were compatible

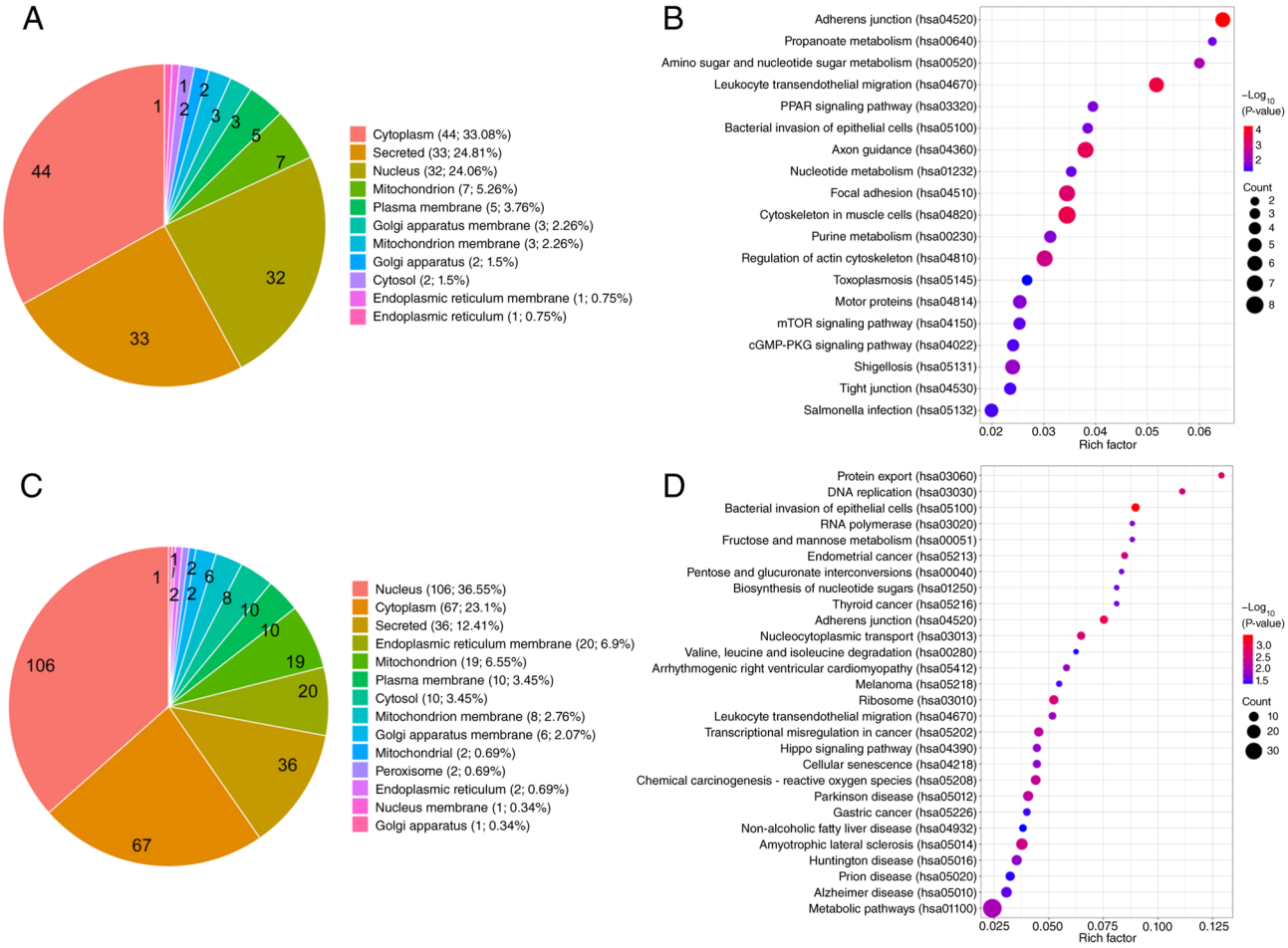

Figure 3. Preliminary characterization of upregulated DAPs in nCRT-resistant tumors. (A) Subcellular localization analysis of the 133 upregulated DAPs in nCRT-resistant tumors before nCRT. (B) Preliminary KEGG pathway enrichment analysis of the 133 upregulated DAPs in nCRT-resistant tumors before nCRT. (C) Subcellular localization analysis of upregulated DAPs in nCRT-resistant tumors after nCRT. (D) Preliminary Kyoto Encyclopedia of Genes and Genomes pathway enrichment analysis of upregulated DAPs in nCRT-resistant tumors after nCRT treatment. DAP, differentially abundant protein; nCRT, neoadjuvant chemoradiotherapy.

with known intrinsic chemo- and radiotherapy-resistance programs, particularly those related to cell-matrix, cell-cell adhesion, cytoskeleton and metabolic adaptation, including 'Adherens junction', 'Focal adhesion', 'Tight junction', 'Regulation of actin cytoskeleton', 'Propanoate metabolism' and 'Amino sugar and nucleotide sugar metabolism'. Myosin regulatory light polypeptide 9 and L1CAM, both more abundant in resistant tumors before nCRT, have previously been associated with worse treatment response or aggressive behavior in CRC and LARC (15,19,35,36). Ribonucleotide reductase regulatory subunit M2, a rate-limiting enzyme for deoxyribonucleotide triphosphates synthesis, has been associated with chemotherapy resistance in CRC (37-39). Glutaryl-CoA dehydrogenase, metastasis-associated colon cancer-1 and 3-phosphoinositide-dependent protein kinase 1 further support a role for pro-tumorigenic signaling and metabolic adaptation in resistant tumors (40-46). Although these observations are descriptive, they suggest that resistant tumors may harbor pre-existing adhesion-associated and metabolic programs before treatment.

Post-nCRT, proteins more abundant in resistant tumors were preliminarily enriched in pathways related to replication, transcription, translation and metabolism, including 'DNA replication', 'RNA polymerase', 'Ribosome', 'Protein export', 'Nucleocytoplasmic transport' and 'Metabolic pathways'. This pattern is compatible with retention of biosynthesis-, replication- and DDR-associated programs in treatment-selected tumors. The increased abundance of MCM family members (MCM2/4/6/7) and RNA polymerase subunits (POLR1E, POLR2E and POLR2I) suggested persistence of replication- and transcription-associated activity (43-45). Elevated expression of the ribosomal protein RPL5 and the mitochondrial ribosomal proteins, MRPL1 and MRPL24, further indicated sustained translational capacity (46,47). Methionyl-tRNA synthetase 1, which has been implicated in DNA damage repair through AIMP3 release and PROM1, a stem cell-associated marker implicated in chemoradiotherapy resistance, were also more abundant in resistant tumors (48-55). In parallel, hexokinase 2 and phosphoribosyl pyrophosphate amidotransferase suggest continued metabolic remodeling, including glycolytic and nucleotide biosynthetic support for treatment-selected cells (56-61). Collectively, these post-treatment data should be interpreted as pathway-level signals consistent with treatment selection rather than direct mechanistic proof of specific resistance processes. In addition, these post-nCRT pathway signals should be interpreted

Table II. Shortlisted upregulated proteins in resistant tumor before therapy.

Gene	Protein accession	P-value	Fold change
BCKDHA	P12694	0.008	2.159
MIOS	Q9NXC5	0.008	1.571
MYL9	P24844	0.013	2.308
L1CAM	P32004	0.049	2.397
RRM2	P31350	0.022	1.553
GCDH	Q92947	0.007	1.648
MACC1	Q6ZN28	0.011	1.702
PDPK1	O15530	0.048	1.263

BCKDHA, branched-chain keto acid dehydrogenase E1 subunit α; MIOS, meiosis regulator for oocyte development; MYL9, myosin light chain 9; L1CAM, L1 cell adhesion molecule; RRM2, ribonucleotide reductase regulatory subunit M2; GCDH, glutaryl-CoA dehydrogenase; MACC1, MET transcriptional regulator MACC1; PDPK1, 3-phosphoinositide dependent protein kinase 1.

Table III. Shortlisted upregulated proteins in resistant tumor post therapy.

Gene	Protein accession	P-value	Fold change
BCKDHA	P12694	0.008	70.848
MIOS	Q9NXC5	0.033	1.546
MCM2	P49736	0.036	1.329
MCM4	P33991	0.009	1.429
MCM6	Q14566	0.043	1.610
MCM7	P33993	0.034	1.669
POLR1E	Q9GZS1	0.047	3.752
POLR2E	P19388	0.008	18.374
POLR2I	P36954	0.047	2.876
RPL5	P46777	0.008	1.279
MRPL1	Q9BYD6	0.008	148.500
MRPL24	Q96A35	0.047	2.674
MARS1	P56192	0.003	1.385
PROM1	O43490	0.045	2.588
HK2	P52789	0.010	1.470
PPAT	Q06203	0.027	2.754

BCKDHA, branched-chain keto acid dehydrogenase E1 subunit α; MIOS, meiosis regulator for oocyte development; MCM2, minichromosome maintenance complex component 2; MCM4, minichromosome maintenance complex component 4; MCM6, minichromosome maintenance complex component 6; MCM7, minichromosome maintenance complex component 7; POLR1E, RNA polymerase I subunit E; POLR2E, RNA polymerase II, I and III subunit E; POLR2I, RNA polymerase II subunit I; RPL5, ribosomal protein L5; MRPL1, mitochondrial ribosomal protein L1; MRPL24, mitochondrial ribosomal protein L24; MARS1, methionyl-tRNA synthetase 1; PROM1, prominin 1; HK2, hexokinase 2; PPAT, phosphoribosyl pyrophosphate amidotransferase.

as bulk tissue readouts of treatment-selected residual lesions rather than as purely tumor-cell-intrinsic changes.

BCKDHA (α subunit), together with BCKDHB (β subunit), form the E1 component of the BCKDH complex. BCKDH consists of E1, E2 (encoded by dihydrolipoamide branched-chain transacylase E2) and E3 (encoded by dihydrolipoamide dehydrogenase) and is the rate-limiting enzyme in branched-chain amino acid (BCAA) catabolism, catalyzing the conversion of BCAAs (leucine, isoleucine and valine) derived intermediates into acetyl-CoA and succinyl-CoA (34). Accumulating evidence has indicated altered BCAA metabolism in CRC (62,63). For example, serum levels of leucine and valine were lower in patients with CRC compared with healthy controls (62). A dynamic metabolomic study of 106 patients with LARC further suggested that BCAA metabolism was associated with response to nCRT, identifying α-ketoisovaleric acid, a key intermediate of BCAA catabolism, as a predictive biomarker and reporting a marked decrease in nCRT resistance in LARC (63). In this context, the consistent direction of higher abundance or expression of BCKDHA across datasets supports prioritizing BCKDHA as a candidate resistance-associated protein. In addition, CRC TMA analysis showed that higher BCKDHA expression was associated with a shorter OS, supporting broader clinical relevance in CRC. However, this TMA cohort addressed prognosis in CRC rather than the pretreatment prediction of nCRT response in LARC; therefore, the TMA findings should be interpreted as supportive rather than definitive evidence of an association between BCKDHA and nCRT response in LARC.

BCAA catabolism can provide tumor cells with energy through the tricarboxylic acid cycle and can also supply carbon and nitrogen for biosynthetic processes, as well as metabolites potentially relevant to epigenomic regulation (64). BCKDHA has been associated with malignant phenotypes in a number of types of cancer, including pancreatic cancer, melanoma and lung cancer; it has been reported to provide carbon for pancreatic cancer cell proliferation (65) and a previous study showed that it promoted melanoma cell malignancy by activating lipogenic enzymes fatty acid synthase and ATP citrate lyase (66). Bo *et al* (67) further demonstrated that X-irradiation induced BCKDHA dephosphorylation in pancreatic and lung cancer cells and that BCKDHA knockdown increased mitotic catastrophe, increased DNA damage and lowered cellular ATP levels. In the present study, BCKDHA overexpression increased clonogenic survival after irradiation, whereas BCKDHA knockdown enhanced radiosensitivity and was accompanied by altered ATM-Chk2-RAD51-associated signaling. Notably, the relatively weak γ-H2AX signal after BCKDHA knockdown did not necessarily exclude persistent DNA damage, as γ-H2AX reflects upstream DDR kinase activity and H2AX availability in addition to double-stranded break burden and the immunoblot readout was not directly equivalent to the γ-H2AX foci assay. A possible explanation lies in BCKDHA-dependent metabolic changes limiting ATP availability, thereby weakening phosphorylation-dependent DDR signaling. The lower ATP levels reported by Bo *et al* (67) were biologically relevant, as ATP not only serves as a cellular

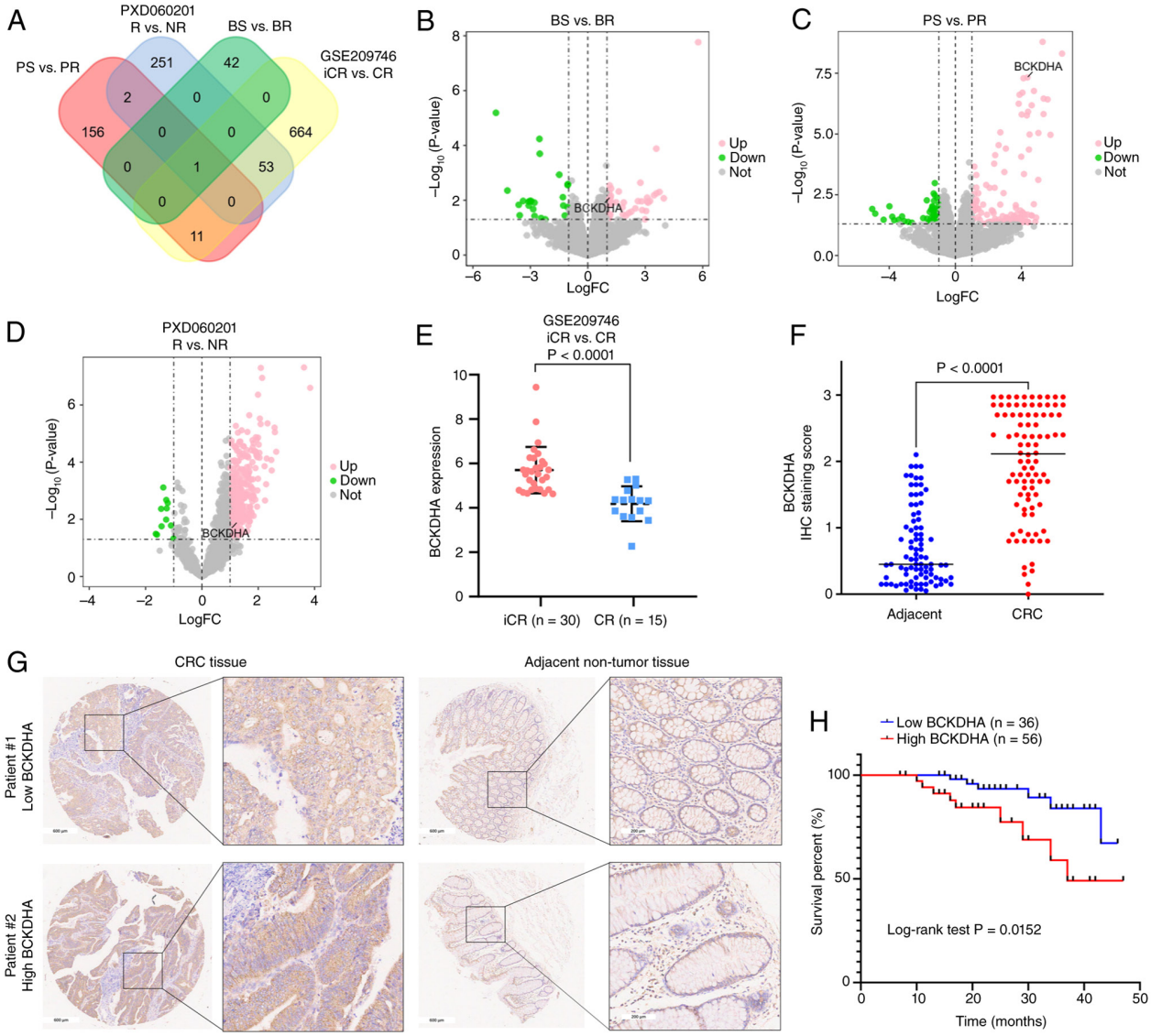

Figure 4. Cross-dataset prioritization of BCKDHA and its broader clinical relevance in CRC. (A) Venn diagram of overlapping potentially associated proteins (P<0.05; $\log_2$FC≥1) among the dataset (BS vs. BR and PS vs. PR), PXD060201 (R vs. NR) and GSE209746 (iCR vs. CR). BCKDHA was identified as a consistently upregulated candidate. Volcano plots of the proteomic data: (B) BS vs. BR and (C) PS vs. PR with BCKDHA labeled. (D) Volcano plot of PXD060201 with BCKDHA labeled. (E) BCKDHA mRNA expression in GSE209746. iCR (n=30) and CR (n=15; P<0.0001). (F) BCKDHA IHC scores in adjacent non-tumor and CRC tissues (P<0.0001). (G) Representative IHC images: low BCKDHA in CRC (left upper panel) and adjacent non-tumor tissue (right upper panel); high BCKDHA in CRC (left lower panel) and adjacent non-tumor tissue (right lower panel). Scale bars, 600 and 200 μm. (H) Kaplan-Meier OS curve of patients with CRC stratified by high BCKDHA expression (n=56) compared with low expression (n=36); log-rank P=0.0152. BCKDHA, branched-chain keto acid dehydrogenase E1 subunit α; CRC, colorectal cancer; nCRT, neoadjuvant chemoradiotherapy; BS, sensitive before nCRT; BR, resistant before nCRT; PS, sensitive post-nCRT; PR, resistant post-nCRT; R, responders; NR, nonresponders; iCR, incomplete response; CR, complete response; IHC, immunohistochemistry; OS, overall survival; FC, fold change; Up, upregulated; Down, downregulated.

energy currency but also as the phosphate donor used by protein kinases. Therefore, reduced ATP availability may contribute to the blunted H2AX phosphorylation observed after BCKDHA knockdown, although the direct molecular association remains to be determined.

A number of limitations of the present study should be noted. First, the proteomic discovery set was small, retrospective, sex-imbalanced and composed of retrospectively screened cases with pelvic MRI available both before and after nCRT and adequate available FFPE material, selected to capture clear RECIST (version 1.1)-defined radiological response categories rather than matched baseline characteristics; this may have increased selection bias and limited reproducibility and generalizability. As the discovery set was markedly sex-imbalanced, potential sex-associated differences in proteomic response patterns could not be evaluated. Second, no proteins remained significant after multiple-testing correction and candidate proteins were screened using nominal P-value and fold-change thresholds. Third, response grouping was based on RECIST rather than pathological regression. Fourth, because no macrodissection or laser-capture microdissection was performed before protein extraction, the post-nCRT FFPE profiles should be interpreted as bulk tissue readouts that may include tumor, stromal, inflammatory and treatment-associated fibrotic components rather than as purely tumor-cell-intrinsic changes. This issue is particularly

Table IV. Correlation between BCKDHA expression and clinicopathological parameters of patients with colorectal cancer.

Variables	All cases (n=92)	BCKDHA expression		P-value
		Low (n=36)	High (n=56)	
Pathology grade				0.386
I-II	58	21	37	
III	34	15	19	
T stage				0.139
T1-3	69	24	45	
T4	23	12	11	
N stage				0.615
N0	43	18	25	
N1-2	49	18	31	
M stage				0.510
M0	84	32	52	
M1	8	4	4	
Sex				0.603
Male	48	20	28	
Female	44	16	28	
Age				0.041[a]
≤65	44	22	22	
>65	48	14	34	

[a]P<0.05. BCKDHA, branched-chain keto acid dehydrogenase E1 subunit α; T, tumor; N, node; M, metastasis.

Table V. Univariate and multivariate Cox proportional hazards regression analysis for overall survival in patients with colorectal cancer.

Variable	Univariate analysis			Multivariate analysis		
	HR	95% CI for HR	P-value	HR	95% CI for HR	P-value
BCKDHA expression high	3.364	1.186-9.539	0.023[a]	2.012	1.122-3.608	0.019[a]
Pathology grade	5.433	1.752-16.854	0.003[b]	5.457	1.684-17.684	0.005[b]
T stage	2.992	1.100-8.136	0.032[a]	3.813	1.023-9.090	0.045[a]
N stage	1.258	0.692-2.287	0.451			
Distant metastasis	0.823	0.108-6.299	0.851			
Sex	0.493	0.178-1.365	0.173			
Age	1.025	0.982-1.070	0.254			

[a]P<0.05; [b]P<0.01. BCKDHA, branched-chain keto acid dehydrogenase E1 subunit α; T, tumor; N, node; HR, hazard ratio.

relevant in post-nCRT specimens, in which treatment can induce fibrosis, inflammation and immune-cell infiltration. Fifth, the CRC tissue microarray addressed broader prognostic relevance in CRC rather than pretreatment predictive value for nCRT response in LARC. Finally, the functional validation was performed primarily in a single cell line and the DDR-associated western blotting data should be interpreted as pathway-level association rather than direct mechanistic proof of DNA repair regulation. Despite these limitations, the present study provides a useful starting point for future research by prioritizing BCKDHA and a number of additional candidate proteins for validation in larger pretreatment LARC cohorts and more direct mechanistic studies.

Collectively, the results of the present study identified BCKDHA as a candidate nCRT resistance-associated protein in LARC, providing preliminary functional evidence linking BCKDHA to the response to radiotherapy and DNA damage response-associated signaling. These findings are hypothesis-generating and warrant validation in larger pretreatment LARC cohorts and in more direct mechanistic studies.

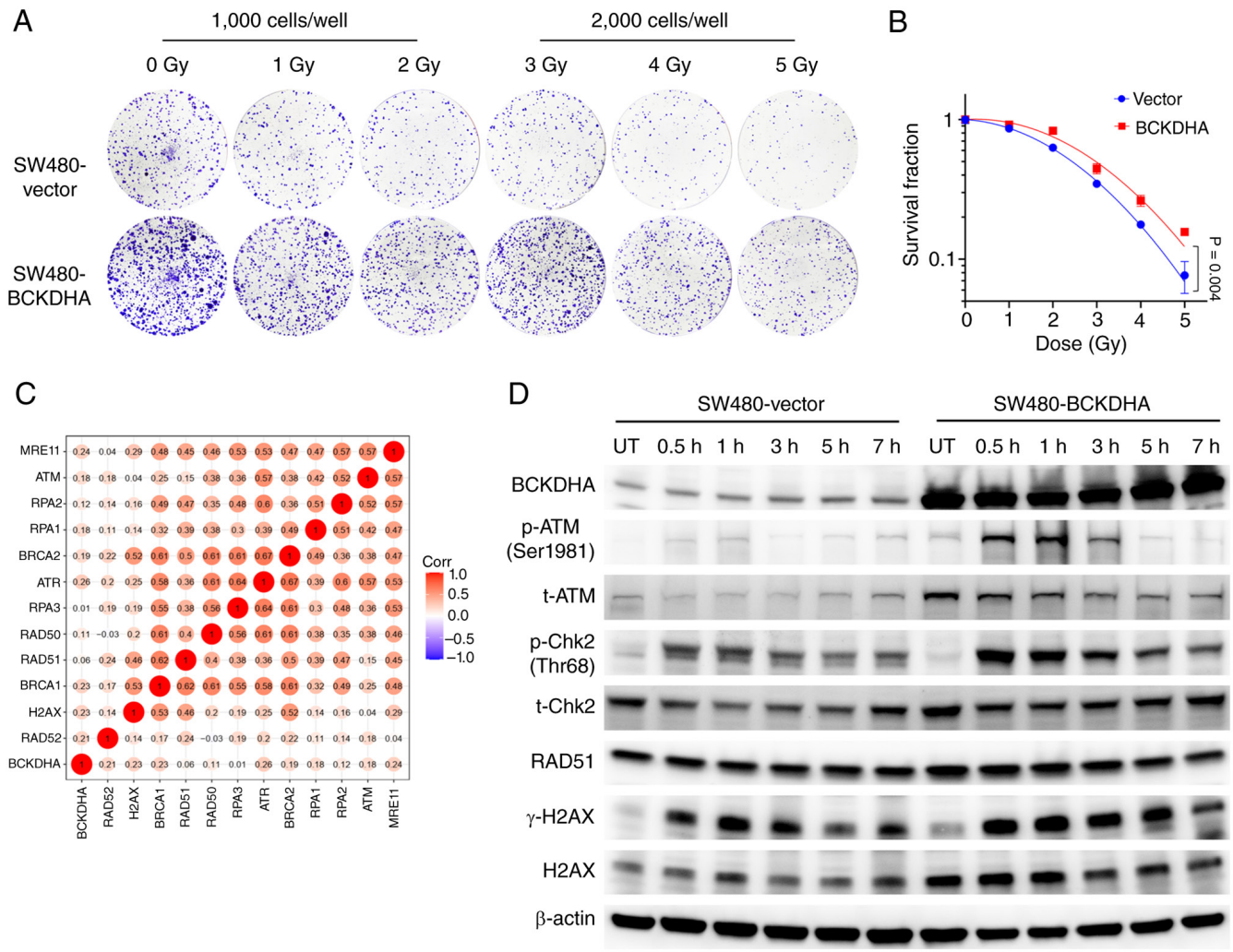

Figure 5. Preliminary functional evidence associating BCKDHA overexpression with the response to radiotherapy and DDR-associated signaling in SW480 cells. Colony formation assay of SW480 cells stably expressing vector control or BCKDHA. Cells were seeded at different densities (1,000 or 2,000 cells per well) to optimize colony formation across a range of irradiation doses (0-5 Gy). (A) Representative images of crystal violet-stained colonies. (B) Survival fraction curves plotted from colony counts. Data are presented as the mean ± SD from three independent experiments (P=0.004 using two-way ANOVA). (C) Spearman correlation analysis between BCKDHA mRNA expression and DDR-associated genes in the GSE209746 dataset. Color intensity indicates correlation coefficient; values labeled on the heatmap represent Spearman's r values. (D) Western blotting analysis of BCKDHA, p-ATM, t-ATM, p-Chk2, t-Chk2, RAD51, γ-H2AX and H2AX in vector control and BCKDHA-overexpressing SW480 cells, UT or at 0.5, 1, 3, 5 and 7 h after 2 Gy X-ray irradiation. β-actin served as a loading control. BCKDHA, branched-chain keto acid dehydrogenase E1 subunit α; DDR, DNA damage response; p, phosphorylated; t, total; ATM, ataxia telangiectasia mutated; Chk2, checkpoint kinase 2; H2AX, H2A histone family member X; UT, untreated; Corr, correlation.

Acknowledgements

Not applicable.

Funding

The present study was supported by the Medical Scientific Research Foundation of Chongqing, China (grant no. 2023MSXM040), the Chongqing Natural Science Foundation General Project (grant no. CSTB2022NSCQ-MSX0773) and the Clinical Study Projects of the First Affiliated Hospital of Army Medical University (grant no. 2024IITZDB11).

Availability of data and materials

The data generated in the present study may be found in the ProteomeXchange consortium via the iProX partner repository under accession number PXD069647 or at the following URL: https://www.iprox.cn/page/subproject.html?id=IPX0013849001.

Authors' contributions

JYH, YDo and CC contributed to the methodology, data acquisition, sample collection, experiments, figure preparation, and writing the original draft. FHL, FWR, QD, YDu and TRL contributed to the experiments and project administration. YYZ, TW and YHC reviewed and verified the clinical data, reviewed and interpreted the experimental data, and designed and performed the X-ray irradiation procedures. XZ, SLX and JJL contributed to conceptualization of the present study, resources, funding acquisition, writing, reviewing and editing the manuscript, and provided supervision. JYH and JJL confirm the authenticity of all the raw data. All authors read and approved the final version of the manuscript.

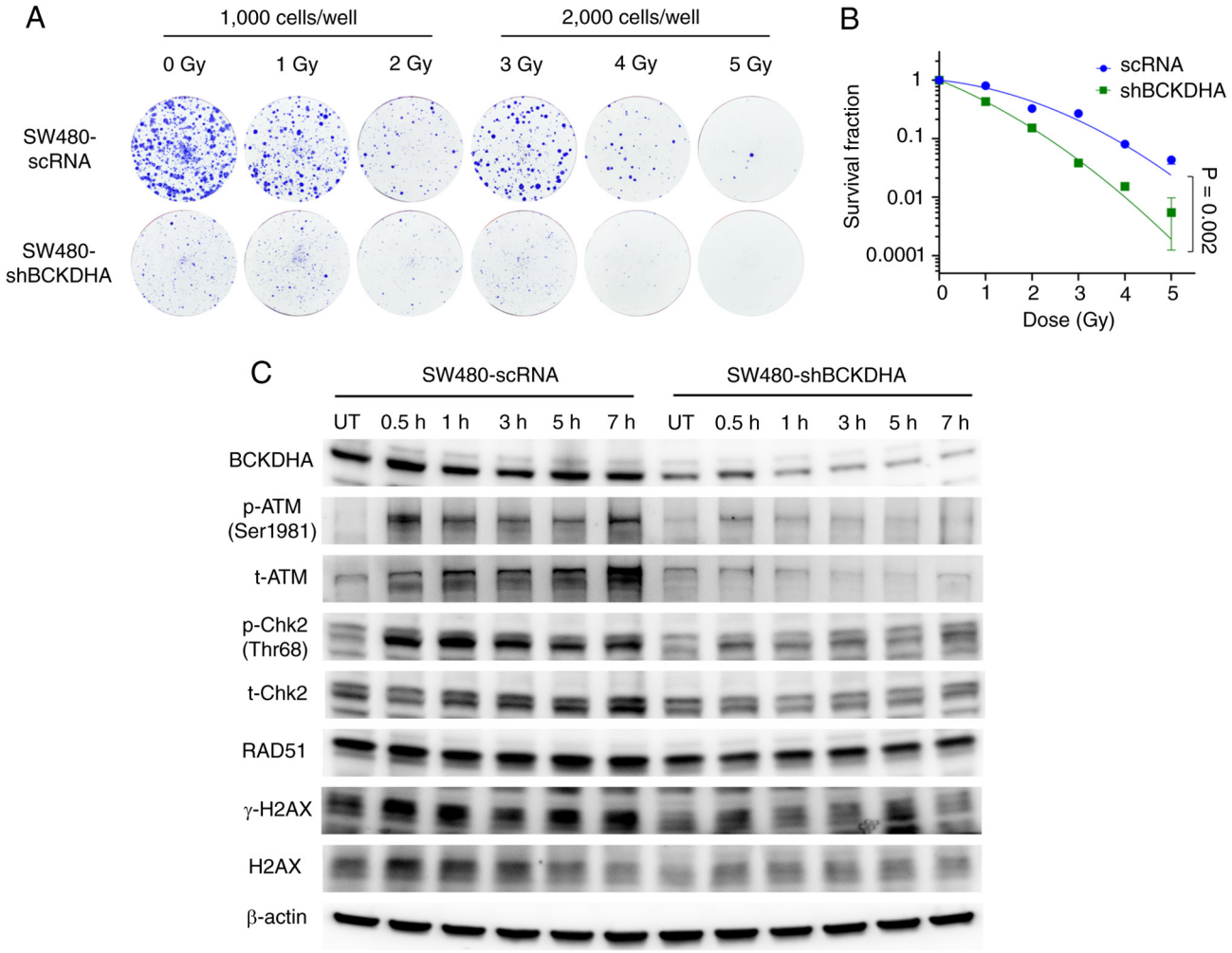

Figure 6. Preliminary functional evidence associating BCKDHA knockdown with increased radiosensitivity and altered DNA damage response-associated signaling in SW480 cells. (A) Representative images of crystal violet-stained colonies of SW480-scRNA and SW480-shBCKDHA cells after 0, 1, 2, 3, 4 and 5 Gy X-ray irradiation. (B) Survival fraction curves plotted from colony counts. Data are presented as the mean ± SD from three independent experiments (P=0.002 using two-way ANOVA). (C) Western blotting analysis of BCKDHA, p-ATM, t-ATM, p-Chk2, t-Chk2, RAD51, γ-H2AX and H2AX in SW480-scRNA and SW480-shBCKDHA cells, UT or at 0.5, 1, 3, 5 and 7 h after 2 Gy X-ray irradiation. β-actin served as a loading control. BCKDHA, branched-chain keto acid dehydrogenase E1 subunit α; scRNA, scrambled RNA; shRNA, short hairpin RNA; ATM, ataxia telangiectasia mutated; Chk2, checkpoint kinase 2; H2AX, H2A histone family member X; UT, untreated; t-, total; p-, phosphorylated.

Ethical approval and consent to participate

The present study protocol was reviewed and approved by the Ethics Committee of the First Affiliated Hospital of Army Medical University, PLA. [approval no. (A)KY2025105]. Written informed consent was obtained from all participants or their legal guardians, where applicable.

Patient consent for publication

Not applicable.

Competing interests

The authors declare that they have no competing interests.

Use of artificial intelligence tools

During the preparation of this work, artificial intelligence tools were used to improve the readability and language of the manuscript or to generate images, and subsequently, the authors revised and edited the content produced by the artificial intelligence tools as necessary, taking full responsibility for the ultimate content of the present manuscript.

References

1. Bray F, Laversanne M, Sung H, Ferlay J, Siegel RL, Soerjomataram I and Jemal A: Global cancer statistics 2022: GLOBOCAN estimates of incidence and mortality worldwide for 36 cancers in 185 countries. CA Cancer J Clin 74: 229-263, 2024.
2. Han B, Zheng R, Zeng H, Wang S, Sun K, Chen R, Li L, Wei W and He J: Cancer incidence and mortality in China, 2022. J Natl Cancer Cent 4: 47-53, 2024.
3. Appelt AL, Pløen J, Harling H, Jensen FS, Jensen LH, Jørgensen JC, Lindebjerg J, Rafaelsen SR and Jakobsen A: High-dose chemoradiotherapy and watchful waiting for distal rectal cancer: A prospective observational study. Lancet Oncol 16: 919-927, 2015.
4. Scott AJ, Kennedy EB, Berlin J, Brown G, Chalabi M, Cho MT, Cusnir M, Dorth J, George M, Kachnic LA, *et al*: Management of locally advanced rectal cancer: ASCO guideline. J Clin Oncol 42: 3355-3375, 2024.

5. Fernandez LM, São Julião GP, Figueiredo NL, Beets GL, van der Valk MJM, Bahadoer RR, Hilling DE, Meershoek-Klein Kranenbarg E, Roodvoets AGH, Renehan AG, *et al*: Conditional recurrence-free survival of clinical complete responders managed by watch and wait after neoadjuvant chemoradiotherapy for rectal cancer in the International Watch & Wait Database: A retrospective, international, multicentre registry study. Lancet Oncol 22: 43-50, 2021.
6. Jin J, Tang Y, Hu C, Jiang LM, Jiang J, Li N, Liu WY, Chen SL, Li S, Lu NN, *et al*: Multicenter, randomized, phase III Trial of Short-term radiotherapy plus chemotherapy versus long-term chemoradiotherapy in locally advanced rectal cancer (STELLAR). J Clin Oncol 40: 1681-1692, 2022.
7. Zhu J, Liu A, Sun X, Liu L, Zhu Y, Zhang T, Jia J, Tan S, Wu J, Wang X, *et al*: Multicenter, randomized, Phase III trial of neoadjuvant chemoradiation with capecitabine and irinotecan guided by UGT1A1 status in patients with locally advanced rectal cancer. J Clin Oncol 38: 4231-4239, 2020.
8. Chang C, Bliggenstorfer JT, Liu J, Shearer J, Dreher P, Bingmer K, Stein SL and Steinhagen E: Not all patients with locally advanced rectal cancer benefit from neoadjuvant therapy. Am Surg 89: 4327-4333, 2023.
9. Couwenberg AM, Burbach JPM, Berbee M, Lacle MM, Arensman R, Raicu MG, Wessels FJ, Verdult J, Roodhart J, Reerink O, *et al*: Efficacy of Dose-escalated chemoradiation on complete tumor response in patients with locally advanced rectal cancer (RECTAL-BOOST): A Phase 2 randomized controlled trial. Int J Radiat Oncol Biol Phys 108: 1008-1018, 2020.
10. Peng J, Lv J and Peng J: KRAS mutation is predictive for poor prognosis in rectal cancer patients with neoadjuvant chemoradiotherapy: A systemic review and meta-analysis. Int J Colorectal Dis 36: 1781-1790, 2021.
11. Kamran SC, Lennerz JK, Margolis CA, Liu D, Reardon B, Wankowicz SA, Van Seventer EE, Tracy A, Wo JY, Carter SL, *et al*: Integrative molecular characterization of resistance to neoadjuvant chemoradiation in rectal cancer. Clin Cancer Res 25: 5561-5571, 2019.
12. Sanz-Garcia E, Argiles G, Elez E and Tabernero J: BRAF mutant colorectal cancer: Prognosis, treatment, and new perspectives. Ann Oncol 28: 2648-2457, 2017.
13. Scott JG, Berglund A, Schell MJ, Mihaylov I, Fulp WJ, Yue B, Welsh E, Caudell JJ, Ahmed K, Strom TS, *et al*: A genome-based model for adjusting radiotherapy dose (GARD): A retrospective, cohort-based study. Lancet Oncol 18: 202-211, 2017.
14. Xia H, Li Z, Lin Y, Lin Y, Zeng L, Xu B, Yao Q and Zheng R: Validation of a genome-based model for adjusting radiotherapy dose (GARD) in patients with locally advanced rectal cancer. Sci Rep 14: 21572, 2024.
15. Chatila WK, Kim JK, Walch H, Marco MR, Chen CT, Wu F, Omer DM, Khalil DN, Ganesh K, Qu X, *et al*: Genomic and transcriptomic determinants of response to neoadjuvant therapy in rectal cancer. Nat Med 28: 1646-1655, 2022.
16. Crotti S, Enzo MV, Bedin C, Pucciarelli S, Maretto I, Del Bianco P, Traldi P, Tasciotti E, Ferrari M, Rizzolio F, *et al*: Clinical predictive circulating peptides in rectal cancer patients treated with neoadjuvant chemoradiotherapy. J Cell Physiol 230: 1822-1828, 2015.
17. Wang H, Ji D, Tian H, Gao Z, Song C, Jia J, Cui X, Zhong L, Shen J and Gu J: Predictive value of proteomic markers for advanced rectal cancer with neoadjuvant chemoradiotherapy. BMC Cancer 22: 868, 2022.
18. Mammano E, Galdi F, Pierobon M, Tessari E, Deng J, Pucciarelli S, Agostini M, De Marchi F, Canzonieri V, De Paoli A, *et al*: Multiplexed protein signal pathway mapping identifies patients with rectal cancer that responds to neoadjuvant treatment. Clin Colorectal Cancer 11: 268-274, 2012.
19. Repetto O, De Re V, De Paoli A, Belluco C, Alessandrini L, Canzonieri V and Cannizzaro R: Identification of protein clusters predictive of tumor response in rectal cancer patients receiving neoadjuvant chemo-radiotherapy. Oncotarget 8: 28328-28341, 2017.
20. Chauvin A, Wang CS, Geha S, Garde-Granger P, Mathieu AA, Lacasse V and Boisvert FM: The response to neoadjuvant chemoradiotherapy with 5-fluorouracil in locally advanced rectal cancer patients: A predictive proteomic signature. Clin Proteomics 15: 16, 2018.
21. Croner RS, Sevim M, Metodiev MV, Jo P, Ghadimi M, Schellerer V, Brunner M, Geppert C, Rau T, Stürzl M, *et al*: Identification of predictive markers for response to neoadjuvant chemoradiation in rectal carcinomas by proteomic isotope coded protein label (ICPL) analysis. Int J Mol Sci 17: 209, 2016.
22. Stanojevic A, Samiotaki M, Lygirou V, Marinkovic M, Nikolic V, Stojanovic-Rundic S, Jankovic R, Vlahou A, Panayotou G, Fijneman RJA, *et al*: Data-Independent acquisition mass spectrometry analysis of FFPE rectal cancer samples offers In-Depth proteomics characterization of the response to neoadjuvant chemoradiotherapy. Int J Mol Sci 24: 15412, 2023.
23. Bowden DL, Sutton PA, Wall MA, Jithesh PV, Jenkins RE, Palmer DH, Goldring CE, Parsons JL, Park BK, Kitteringham NR and Vimalachandran D: Proteomic profiling of rectal cancer reveals acid ceramidase is implicated in radiation response. J Proteomics 179: 53-60, 2018.
24. Babic T, Lygirou V, Rosic J, Miladinov M, Rom AD, Baira E, Stroggilos R, Pappa E, Zoidakis J, Krivokapic Z and Nikolic A: Pilot proteomic study of locally advanced rectal cancer before and after neoadjuvant chemoradiotherapy indicates high metabolic activity in non-responders' tumor tissue. Proteomics Clin Appl 17: e2100116, 2023.
25. Zott T, Wolf M, Plessl-Walder G, Regele H, Bergmann M, Meier-Menches SM, Gerner C, Silberhumer GR and Bileck A: Proteomic analysis of FFPE tissue samples identifies potential molecular mechanisms mediating resistance to radiotherapy in rectal cancer. J Proteome Res 24: 3990-4001, 2025.
26. Weiser MR: AJCC 8th Edition: Colorectal Cancer. Ann Surg Oncol 25: 1454-1455, 2018.
27. R Core Team. R: A language and environment for statistical computing. Vienna, Austria: R Foundation for Statistical Computing, 2012.
28. Thévenot EA, Roux A, Xu Y, Ezan E and Junot C: Analysis of the human adult urinary metabolome variations with age, body mass index and gender by implementing a comprehensive workflow for univariate and OPLS statistical analyses. J Proteome Res 14: 3322-3335, 2015.
29. Wickham H: ggplot2: Elegant Graphics for Data Analysis. Springer-Verlag New York, New York, NY, 2016.
30. Kolde R: pheatmap: Pretty Heatmaps. R package version 1.0.12, 2019. Available from: https://CRAN.R-project.org/package=pheatmap.
31. Goldberg T, Hecht M, Hamp T, Karl T, Yachdav G, Ahmed N, Altermann U, Angerer P, Ansorge S, Balasz K, *et al*: LocTree3 prediction of localization. Nucleic Acids Res 42: W350-W355, 2014.
32. Kanehisa M: Post-genome Informatics: Oxford University Press, 2000.
33. Wang HB, Zhang H, Zhang JP, Li Y, Zhao B, Feng GK, Liu W, Li MZ, Huang WL, Tsao SW, *et al*: Neuropilin 1 is an entry factor that promotes EBV infection of nasopharyngeal epithelial cells. Nat Commun 6: 6240, 2015.
34. Peng H, Wang Y and Luo W: Multifaceted role of branched-chain amino acid metabolism in cancer. Oncogene 39: 6747-6756, 2020.
35. Deng S, Cheng D, Wang J, Gu J, Xue Y, Jiang Z, Qin L, Mao F, Cao Y and Cai K: MYL9 expressed in cancer-associated fibroblasts regulate the immune microenvironment of colorectal cancer and promotes tumor progression in an autocrine manner. J Exp Clin Cancer Res 42: 294, 2023.
36. Ganesh K, Basnet H, Kaygusuz Y, Laughney AM, He L, Sharma R, O'Rourke KP, Reuter VP, Huang YH, Turkekul M, *et al*: L1CAM defines the regenerative origin of metastasis-initiating cells in colorectal cancer. Nat Cancer 1: 28-45, 2020.
37. Zhan Y, Jiang L, Jin X, Ying S, Wu Z, Wang L, Lou Y and Qiu Y: Inhibiting RRM2 to enhance the anticancer activity of chemotherapy. Biomed Pharmacother 133: 110996, 2021.
38. Yazdanian Z, Mobarra N, Fazel A, Fazeli MS, Ghasemi S, Danesteh S, Khoshrou A, Pakzad R, Raji S, Rafiee M and Akbar S: Ribonucleotide-diphosphate reductase subunit M2 (RRM2) expression and colorectal cancer invasiveness: A potential prognostic biomarker. Mol Biol Rep 52: 447, 2025.
39. Lin ZP, Belcourt MF, Cory JG and Sartorelli AC: Stable suppression of the R2 subunit of ribonucleotide reductase by R2-targeted short interference RNA sensitizes p53(-/-) HCT-116 colon cancer cells to DNA-damaging agents and ribonucleotide reductase inhibitors. J Biol Chem 279: 27030-27038, 2004.
40. Verma S, Crawford D, Khateb A, Feng Y, Sergienko E, Pathria G, Ma CT, Olson SH, Scott D, Murad R, *et al*: NRF2 mediates melanoma addiction to GCDH by modulating apoptotic signalling. Nature Cell Biology 24: 1422-1432, 2022.
41. Radhakrishnan H, Walther W, Zincke F, Kobelt D, Imbastari F, Erdem M, Kortüm B, Dahlmann M and Stein U: MACC1-the first decade of a key metastasis molecule from gene discovery to clinical translation. Cancer Metastasis Rev 37: 805-820, 2018.

42. Han D, Wang W, Jeon JH, Shen T, Huang X, Yi P, Dong B and Yang F: Cooperative activation of PDK1 and AKT by MAPK4 enhances cancer growth and resistance to therapy. PLoS Biol 21: e3002227, 2023.
43. Tian Y, Zhou Y, Chen F, Qian S, Hu X, Zhang B and Liu Q: Research progress in MCM family: Focus on the tumor treatment resistance. Biomed Pharmacother 173: 116408, 2024.
44. Malysa A, Zhang XM and Bepler G: Minichromosome maintenance proteins: From DNA replication to the DNA damage response. Cells 14: 12, 2024.
45. Muste Sadurni M and Saponaro M: Deregulations of RNA Pol II subunits in cancer. Appl Biosci 2: 459-476, 2023.
46. El Khoury W and Nasr Z: Deregulation of ribosomal proteins in human cancers. Biosci Rep 41: BSR20211577, 2021.
47. Lin X, Guo L, Lin X, Wang Y and Zhang G: Expression and prognosis analysis of mitochondrial ribosomal protein family in breast cancer. Sci Rep 12: 10658, 2022.
48. Khan K, Gogonea V and Fox PL: Aminoacyl-tRNA synthetases of the multi-tRNA synthetase complex and their role in tumorigenesis. Transl Oncol 19: 101392, 2022.
49. Jin Q, Liu G, Wang B, Li S, Ni K, Wang C, Ren J, Zhang S and Dai Y: High methionyl-tRNA synthetase expression predicts poor prognosis in patients with breast cancer. J Clin Pathol 73: 803-812, 2020.
50. Jang SI, Nahm JH, Lee SY, Cho JH, Do MY, Park JS, Lee HS, Yang J, Kong J, Jung S, *et al*: Prediction of prognosis in pancreatic cancer according to Methionyl-tRNA synthetase 1 expression as determined by immunohistochemical staining. Cancers (Basel) 15: 5413, 2023.
51. Kwon NH, Kang T, Lee JY, Kim HH, Kim HR, Hong J, Oh YS, Han JM, Ku MJ, Lee SY and Kim S: Dual role of methionyl-tRNA synthetase in the regulation of translation and tumor suppressor activity of aminoacyl-tRNA synthetase-interacting multifunctional protein-3. Proc Natl Acad Sci USA 108: 19635-19640, 2011.
52. Ren F, Sheng WQ and Du X: CD133: A cancer stem cells marker, is used in colorectal cancers. World J Gastroenterol 19: 2603-2611, 2013.
53. Zhang X, Yang L, Lei W, Hou Q, Huang M, Zhou R, Enver T and Wu S: Single-cell sequencing reveals CD133+CD44-originating evolution and novel stemness related variants in human colorectal cancer. EBioMedicine 82: 104125, 2022.
54. Yuan Z, Liang X, Zhan Y, Wang Z, Xu J, Qiu Y, Wang J, Cao Y, Le VM, Ly HT, *et al*: Targeting CD133 reverses drug-resistance via the AKT/NF-κB/MDR1 pathway in colorectal cancer. Br J Cancer 122: 1342-1353, 2020.
55. Akbari M, Shomali N, Faraji A, Shanehbandi D, Asadi M, Mokhtarzadeh A, Shabani A and Baradaran B: CD133: An emerging prognostic factor and therapeutic target in colorectal cancer. Cell Biol Int 44: 368-380, 2020.
56. Liao M, Yao D, Wu L, Luo C, Wang Z, Zhang J and Liu B: Targeting the Warburg effect: A revisited perspective from molecular mechanisms to traditional and innovative therapeutic strategies in cancer. Acta Pharm Sin B 14: 953-1008, 2024.
57. Huang X, Liu M, Sun H, Wang F, Xie X, Chen X, Su J, He Y, Dai Y, Wu H and Shen L: HK2 is a radiation resistant and independent negative prognostic factor for patients with locally advanced cervical squamous cell carcinoma. Int J Clin Exp Pathol 8: 4054-4063, 2015.
58. Barba I, Carrillo-Bosch L and Seoane J: Targeting the warburg effect in cancer: Where Do We Stand? Int J Mol Sci 25: 3142, 2024.
59. Pareek V, Pedley AM and Benkovic SJ: Human de novo purine biosynthesis. Crit Rev Biochem Mol Biol 56: 1-16, 2021.
60. Kodama M, Oshikawa K, Shimizu H, Yoshioka S, Takahashi M, Izumi Y, Bamba T, Tateishi C, Tomonaga T, Matsumoto M and Nakayama KI: A shift in glutamine nitrogen metabolism contributes to the malignant progression of cancer. Nat Commun 11: 1320, 2020.
61. Zhou W and Wahl DR: Purine metabolism promotes radioresistance and is a therapeutic target in glioblastoma. Mol Cell Oncol 7: 1834902, 2020.
62. Qiu Y, Cai G, Su M, Chen T, Zheng X, Xu Y, Ni Y, Zhao A, Xu LX, Cai S and Jia W: Serum metabolite profiling of human colorectal cancer using GC-TOFMS and UPLC-QTOFMS. J Proteome Res 8: 4844-4850, 2009.
63. Lv J, Jia H, Mo M, Yuan J, Wu Z, Zhang S, Zhe F, Gu B, Fan B, Li C, *et al*: Changes of serum metabolites levels during neoadjuvant chemoradiation and prediction of the pathological response in locally advanced rectal cancer. Metabolomics 18: 99, 2022.
64. Sivanand S and Vander Heiden MG: Emerging roles for Branched-chain amino acid metabolism in cancer. Cancer Cell 37: 147-156, 2020.
65. Lee JH, Cho YR, Kim JH, Kim J, Nam HY, Kim SW and Son J: Branched-chain amino acids sustain pancreatic cancer growth by regulating lipid metabolism. Exp Mol Med 51: 1-11, 2019.
66. Tian Y, Ma J, Wang M, Yi X, Guo S, Wang H, Zhang H, Wang H, Yang Y, Zhang B, *et al*: BCKDHA contributes to melanoma progression by promoting the expressions of lipogenic enzymes FASN and ACLY. Exp Dermatol 32: 1633-1643, 2023.
67. Bo T, Osaki T and Fujii J: Dephosphorylation of branched-chain α-keto acid dehydrogenase E1α (BCKDHA) promotes branched-chain amino acid catabolism and renders cancer cells resistant to X-rays by mitigating DNA damage. Biochem Biophys Res Commun 742: 151154, 2025.

Copyright © 2026 He et al. This work is licensed under a Creative Commons Attribution-NonCommercial-NoDerivatives 4.0 International (CC BY-NC-ND 4.0) License.